

Dissociation mechanism of $C_2H_4^{2+}$ induced by 18-keV/u Ne^{8+} impact: Symmetric and isomeric cleavage of the C-C bond

Baihui Ren ¹, Pufang Ma,¹ Yu Zhang ^{2,*}, Long Wei ¹, Jie Han,¹ Zihan Xia,¹ Jiarong Wang,¹ Tianming Meng,¹ Wandong Yu ³, Yaming Zou,¹ Chuan-Lu Yang,^{4,†} and Baoren Wei ^{1,‡}

¹*Institute of Modern Physics, Key Laboratory of Nuclear Physics and Ion-Beam Application (MOE), Fudan University, Shanghai 200433, China*

²*College of Data Science, Jiaying University, Jiaying 314001, China*

³*State Key Laboratory for Mesoscopic Physics and Frontiers Science Center for Nano-Optoelectronics, School of Physics, Peking University, Beijing 100871, China*

⁴*School of Physics and Optoelectronics Engineering, Ludong University, Yantai 264025, China*



(Received 13 April 2022; accepted 24 June 2022; published 11 July 2022)

The C-C bond cleavage dissociation of ethylene dication produced by 18-keV/u Ne^{8+} impact is investigated by combining experimental measurement and theoretical calculation. Using cold target recoil ion momentum spectroscopy, two channels, i.e., the symmetric fragmentation, $C_2H_4^{2+} \rightarrow CH_2^+ + CH_2^+$, and the isomeric one, $C_2H_4^{2+} \rightarrow CH^+ + CH_3^+$, are clearly identified and thus their kinetic-energy release (KER) distributions are determined. The average KER values are then compared with the theoretical results obtained by quantum chemical calculations, which provide reaction paths of both channels on the potential-energy surfaces of different molecular states. It is found that the hydrogen transfer process and excited-state dynamics still play crucial roles in the formation of C-C bond cleavage channels, but in a different way in comparison with the cases of acetylene C_2H_2 and ethane C_2H_6 .

DOI: [10.1103/PhysRevA.106.012805](https://doi.org/10.1103/PhysRevA.106.012805)

I. INTRODUCTION

Understanding the underlying electronic and nuclear dynamics of polyatomic molecules ionized by energetic particle collisions provides elementary knowledge of the fields of, e.g., controlled chemical reactions [1], plasma physics [2], and radiation damage [3]. During collisions, the bound electrons of a molecule could be excited and ionized. The ultrafast electronic migration will trigger nuclear motion, which leads to molecular fragmentation if enough internal energy is available [4,5]. The fragmentation can occur directly, e.g., rapid Coulomb explosion [6], as long as the chemical bond involved continuously elongates and finally breaks up. In addition to the dominant direct fragmentation, there is another kind of path involving chemical bond rearrangement and isomerization prior to the final fragmentation. The isomeric dissociation is usually low yielding but presents unique and interesting dynamics. For example, the intramolecular-hydrogen-transfer induced isomerization has been extensively studied for its key role in biologically functional complexes [7–9]. To probe the isomerization dynamics during the collision-induced dissociation, the coincident three-dimensional momentum imaging technique, e.g., cold target recoil ion momentum spectroscopy (COLTRIMS) [10], is generally employed.

Due to the high mobility of light-mass hydrogen atoms, hydrocarbon molecules have been chosen as essential prototypes to study isomerization and corresponding fragmentation processes. The hydrogen atoms can migrate along the C-C skeletal bonds and cause various important chemical reactions [11], e.g., 1,2-hydrogen shift and roaming processes. These processes have been extensively investigated by intense laser field ionization [12–18], which enables precise measurement of temporal and energetic information. However, strong laser pulses with rather long irradiation times could easily alter the profile of the molecular potential-energy surface (PES). In contrast, the ion-molecule collision has a short interaction time and thus provides a more direct scheme to uncover the isomerization mechanism [19–26]. On the theoretical side, PES calculation is pertinent to the identification of the fragmentation mechanism by tracing a series of intermediates and transition states in reaction paths [27,28].

As two of the simplest hydrocarbon molecules, acetylene and ethane have attracted much attention for their C-C bond cleavage dissociation [12–16,22,24,29,30]. Both the direct or symmetric fragmentation channel ($C_2H_{2n}^{2+} \rightarrow CH_n^+ + CH_n^+$) ($n = 1, 3$) and the isomeric or asymmetric one ($C_2H_{2n}^{2+} \rightarrow CH_{(n+1)}^+ + CH_{(n-1)}^+$) ($n = 1, 3$) are observed in the dication dissociation. The latter channel concerns the ultrafast hydrogen transfer on tens of femtosecond timescales [12–14]. The asymmetric fragmentation of $C_2H_6^{2+}$ has a single-peaked kinetic-energy release (KER) distribution and is considered to occur on the PES of the excited state, i.e., the lowest triplet

*zyclay@outlook.com

†ycl@ldu.edu.cn

‡brwei@fudan.edu.cn

one [24]. However, the KER distribution of $C_2H_2^{2+}$ asymmetric fragmentation is bimodal and involves isomerization on the PES of some higher excited states [22,27,30]. For the symmetric fragmentation, the hydrogen transfer process is not involved in the C-C bond cleavage of $C_2H_2^{2+}$ [15,27], but it is an important contributor to the case of $C_2H_6^{2+}$ [16,24]. A considerable proportion of the parent ion $[CH_3 - CH_3]^{2+}$ could be isomerized to the intermediate of $[CH_2 - CH_4]^{2+}$ by hydrogen transfer and finally dissociated into two CH_3^+ fragments from the double bridge structure $[H_2C(H_2)CH_2]^{2+}$. So the $C_2H_6^{2+}$ symmetric channel has a rather complicated reaction path as compared to the one-step dissociation of the $C_2H_2^{2+}$ case. And for each symmetric channel, both the ground and excited states contribute to the features of KER distribution [22,24,29,30]. As mentioned above, the hydrogen transfer process and excited-state dynamics have significant effects on the C-C bond cleavage of acetylene and ethane molecules, but in different ways. Therefore, to better understand their roles, another molecule with the C-C bond, i.e., ethylene, occupying the middle ground between acetylene and ethane could be studied.

In this paper, we report the C-C bond cleavage dissociation dynamics of ethylene dication produced by 18-keV/u Ne^{8+} impact. The symmetric and isomeric channels, i.e., $C_2H_4^{2+} \rightarrow CH_2^+ + CH_2^+$ and $CH^+ + CH_3^+$, are identified and measured utilizing the COLTRIMS technique. Revolving around the experimental KER distributions of both channels, *ab initio* quantum chemical calculations are carried out to obtain reaction paths of $C_2H_4^{2+}$ in singlet and triplet states. The roles of hydrogen transfer and excited state in the formation of symmetric and asymmetric fragmentation will be examined.

II. METHODS

The collision-induced dissociation experiment was carried out using the COLTRIMS setup at Fudan University. The details of the setup have been described before [31]. Briefly, a beam of 18-keV/u Ne^{8+} ions produced by an electron cyclotron resonance ion source was guided to a high vacuum collision chamber and therein perpendicularly collided with a supersonic jet of ethylene gas. The resultant ionic species were extracted and accelerated by a uniform electrostatic field of 100 V/cm, and projected to a position-sensitive detector (PSD). The PSD consisted of double microchannel plates and a delay-line anode, which was mounted at the end of a Wiley-McLaren time-of-flight (TOF) tube. After the interaction, the scattered ions had different charge states due to charge exchange. They were separated by an electrostatic deflector, and finally hit on another PSD. According to the TOF and position data from the PSD, three-dimensional-momentum vectors of the recoil ions were reconstructed. And thus the KER of each coincident channel could be deduced as the kinetic-energy sum of all fragments in this channel. In particular, for the two-body channels studied here, the KER in the center-of-mass coordinate system could be obtained. Thus we did not need to consider the influence of the projectile momentum transfer, which could induce recoil energy of the fragments. This energy was estimated to be about tens of meV by the

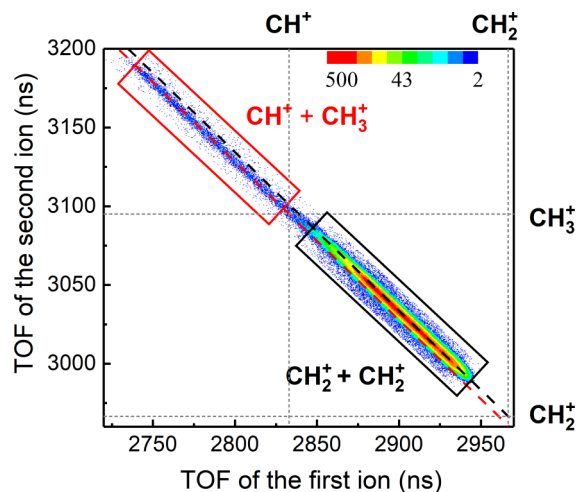


FIG. 1. Ion-ion coincidence TOF map of the overlapped two-body fragmentation channels $CH_2^+ + CH_2^+$ and $CH^+ + CH_3^+$ of the $C_2H_4^{2+}$ ion caused by 18-keV/u Ne^{8+} impact. The areas surrounded by black and red rectangles are analyzed for $CH_2^+ + CH_2^+$ and $CH^+ + CH_3^+$, respectively. The red and black dashed lines are drawn with a slope of -1 , and through the nominal TOFs of (CH^+, CH_3^+) and (CH_2^+, CH_2^+) .

measured results of [32] and much smaller than the fragment energy due to a pure Coulomb explosion. To exclude the random coincidence events, the center-of-mass momentum sum of two coincidence fragments was limited to lie between ± 5 a. u. in each direction. The measurements were calibrated by the Coulomb explosion kinematics of N_2 dication under the same experimental condition. In the present paper, both the transfer ionization and double capture mechanisms (corresponding to Ne^{7+} and Ne^{6+} scattered projectiles, respectively) contributed to the studied channels, whereas the former is dominant with a relative importance of about 85%. And there is no obvious difference in the structure of the KER distribution in the cases of Ne^{7+} and Ne^{6+} . Thus during the data analysis, we did not separate the scattered projectiles.

The dissociative reaction paths of $C_2H_4^{2+}$ dication were searched on the PESs of singlet and triplet states using the GAUSSIAN 16 package [33]. Employing the density functional theory with the B3LYP functional and aug-cc-pVTZ basis set, geometry optimization and single-point energy calculation were performed for initial $C_2H_4^{2+}$ ions, intermediate (INT), transition state (TS), and products. Zero-point energy (ZPE) corrections were included. To ensure the connection between a TS and corresponding reactant, INT, or products, intrinsic reaction coordinate (IRC) calculations were carried out at the same theoretical level. In each reaction path, the reverse activation energy, i.e., the energy difference between the highest TS and products, could be released as the kinetic energy of products. And this energy was compared to the experimental KER value of the corresponding channel.

III. RESULTS AND DISCUSSION

Figure 1 displays a partial TOF correlation map of two-body fragmentation channels of the $C_2H_4^{2+}$ ion induced by

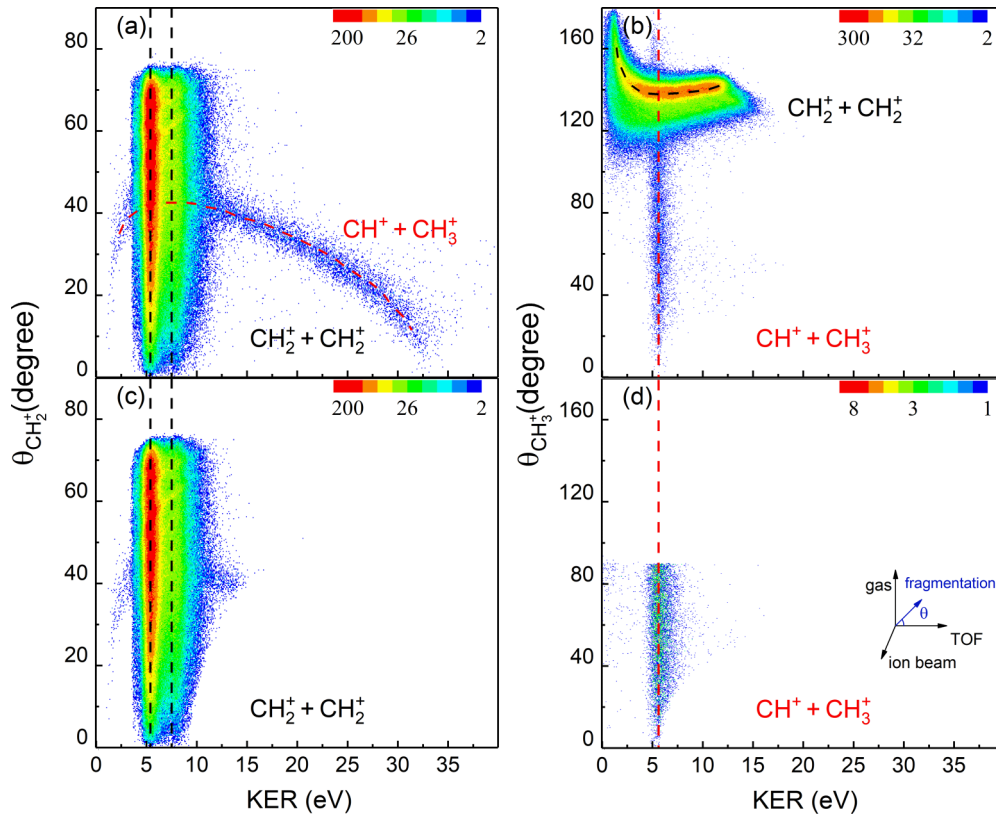


FIG. 2. (a) KER- $\theta_{CH_2^+}$ and (b) KER- $\theta_{CH_3^+}$ coincidence maps for all of the events in Fig. 1. The $\theta_{CH_2^+}$ and $\theta_{CH_3^+}$ represent the dissociation angle between the fragmentation direction and TOF axis for $CH_2^+ + CH_2^+$ and $CH^+ + CH_3^+$ channels, respectively. (c) KER- $\theta_{CH_2^+}$ map for the fragmentation events in the black rectangle in Fig. 1. (d) KER- $\theta_{CH_3^+}$ map for the events in the red rectangle in Fig. 1.

Ne^{8+} projectile. The abscissa is the TOF of the first hitting ion while the ordinate is that of the second one. In consequence of momentum conservation, the two-body fragmentation should be shown with a slope of -1 . The parallel black and red dashed lines are added with a slope of -1 to help identify the fragmentation channels. In the eye-catching long island, there are two data structures surrounded by black and red rectangles, respectively. As shown in Fig. 1, the black dashed line passes through both the nominal TOFs of (CH_2^+ , CH_2^+) and the axis of symmetry of the lower part, which is a sign that the events inside the black rectangle are mainly contributed by the fragmentation channel $CH_2^+ + CH_2^+$. Likewise, the events within the red rectangle could be identified utilizing the red dashed line, and are considered to result from the $CH^+ + CH_3^+$ ion pair. Thus, according to the TOF, the two two-body fragmentation channels in Fig. 1 are preliminarily identified; one is a symmetric process with direct cleavage of the C-C bond and the other is an asymmetric dissociation channel initiated by hydrogen-transfer-induced isomerization, as shown below:



However, as shown in Fig. 1, these two channels are overlapped in the TOF domain and cannot be completely separated from each other under the present experimental condition.

This is mainly due to the proximity of the mass-to-charge ratio of the above fragments (CH^+ , CH_2^+ , and CH_3^+) and the broadening of their TOFs.

To further disentangle them and obtain the branching ratios of the overlapped channels, the correlation map of KER distribution versus dissociation angle is analyzed, as shown in Fig. 2. A detailed description of the analysis method has been presented before [30], and only a brief introduction is given here. Herein, since the two fragments fly in opposite directions in the two-body fragmentation, we define the angle between the momentum of one of the fragments and the TOF axis as the dissociation angle θ ($\theta_{CH_2^+}$ and $\theta_{CH_3^+}$). In the present experiment, due to the random orientation of target molecules, either of the fragments in a two-body fragmentation is usually emitted isotropically. The KER distribution of the fragmentation channel is independent of the dissociation angle and should be distributed vertically in the KER- θ map of the corresponding channel. Assuming the coincidence events in Fig. 1 are totally contributed by the fragmentation channel I or channel II, the KER- $\theta_{CH_2^+}$ and KER- $\theta_{CH_3^+}$ correlation maps are presented in Figs. 2(a) and 2(b). As shown in Fig. 2(a), there are two distinct structures, the main one along the vertical black dashed lines and the minor one along the red dashed curve. The KER of events around the vertical line is independent of $\theta_{CH_2^+}$, indicating that the events originate from channel I. The events around the red curve, however, show a peculiar dependence on the dissociation angle, which is caused by the misjudgment of channel identification, and

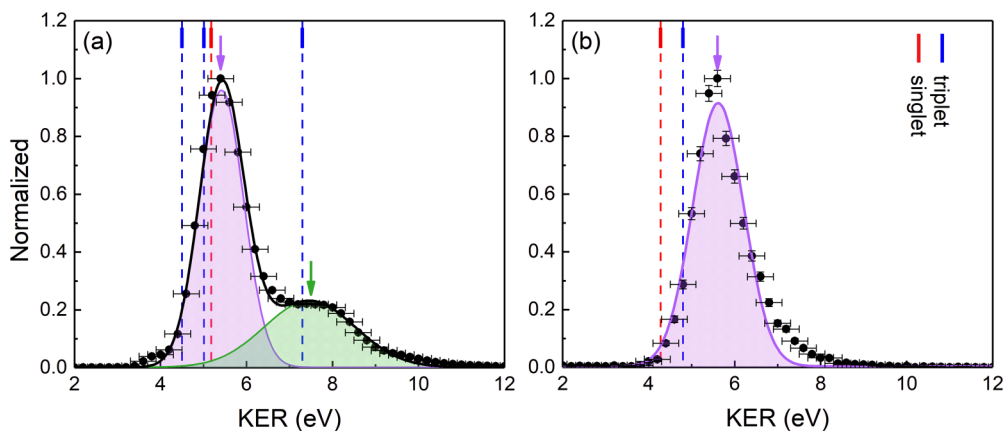


FIG. 3. Kinetic-energy release distributions for fragmentation channels (a) $\text{CH}_2^+ + \text{CH}_2^+$ and (b) $\text{CH}^+ + \text{CH}_3^+$. The black, purple, and green solid lines correspond to the Gaussian-fitting profiles. The purple and green arrows mark the peaks of the Gaussian fit. The red and blue vertical bars with dashed lines represent theoretical values obtained by reaction path calculations for the singlet and triplet states, respectively.

these events should correspond to channel II. Similar features are observed in Fig. 2(b); the events distributed along the red vertical dashed line are attributed to channel II, while those along the curved dashed line correspond to channel I. Based on the above analysis, we separately plot KER- θ correlation maps of the events in the red and black rectangles (in Fig. 1) as shown in Figs. 2(c) and 2(d). The KER distribution of events in Fig. 2(c) [Fig. 2(d)] is parallel to the $\theta_{\text{CH}_2^+}$ ($\theta_{\text{CH}_3^+}$) axis, which is totally from channel I (channel II), reconfirming the decoupling of fragmentation channels I and II.

The isotropy of dissociation angle means a sinusoidal distribution in the range of 0° – 180° . The angle distribution of channel I in Figs. 2(a) and 2(c) is from 0° to $\sim 80^\circ$, mainly caused by the identity of the two CH_2^+ fragments and the detector dead time. For channel II in Fig. 2(b), a complete angle distribution (from 0° to 180°) is displayed. But the dissociation angle in Fig. 2(d) is only distributed from 0° to $\sim 90^\circ$ because nearly half of the events in channel II are mixed with channel I [see Fig. 2(b)]. Consequently, when extracting the branching ratios of the two channels, both $\theta_{\text{CH}_2^+}$ and $\theta_{\text{CH}_3^+}$ are limited to less than 30° to avoid the influence of detector dead time and the overlap of the two channels. As a result of two identical fragments in channel I, only half of the event counts are considered actual. In this way, the branching ratios of channels I and II are estimated to be 98.7 and 1.3% with a margin of error of about 15%, which is mainly from the detection efficiency and statistical errors.

For fragmentation channels I and II, the KER distributions are deduced from the momenta of corresponding fragment ion pairs and shown in Figs. 3(a) and 3(b), respectively. The black dots are the measured KER distributions. The uncertainties presented as horizontal and vertical error bars are mainly from the momentum uncertainty of 0.3 eV and the data statistics. The large distribution of impact parameters in ion-molecule collisions causes a wide electronic and vibrational energy transfer and thus leads to a broad KER distribution. A broad asymmetric bimodal KER distribution is obtained for the symmetric fragmentation channel I, as shown in Fig. 3(a). Through a double-Gaussian fitting, it is measured to peak at around 5.4 eV with a higher-energy contribution at around 7.5 eV. Since the KER distribution is closely related to the

molecular potential-energy surface, these two structures indicate at least two energy transfer paths during the direct cleavage of the C-C bond. In Fig. 3(b), the KER distribution for the isometric fragmentation channel II shows a nearly unimodal distribution with a peak around 5.6 eV. In order to further explain these KER values and explore the underlying mechanisms of the symmetric and isomeric fragmentation channels, we have performed the *ab initio* reaction path calculations on the PES of $\text{C}_2\text{H}_4^{2+}$ singlet and triplet states, as shown in Figs. 4 and 5. The theoretical level of B3LYP/aug-cc-pVTZ is employed for all calculations including geometry optimization, single-point energy, ZPE correction, and IRC calculation.

As shown in Fig. 4, for the $\text{CH}_2^+ + \text{CH}_2^+$ channel, one reaction path from the singlet state and three from the triplet state are obtained through searching corresponding PESs. All of those paths exhibit a one-step dissociation with a productlike transition state. It is patently obvious that the 1,2-hydrogen shift does not come into the symmetric fragmentation, which is the case for $\text{C}_2\text{H}_2^{2+}$ [15,27], but not for $\text{C}_2\text{H}_6^{2+}$ [24]. After vertical double ionization, the $\text{C}_2\text{H}_4^{2+}$ ion in the singlet state relaxes to a global minimum with

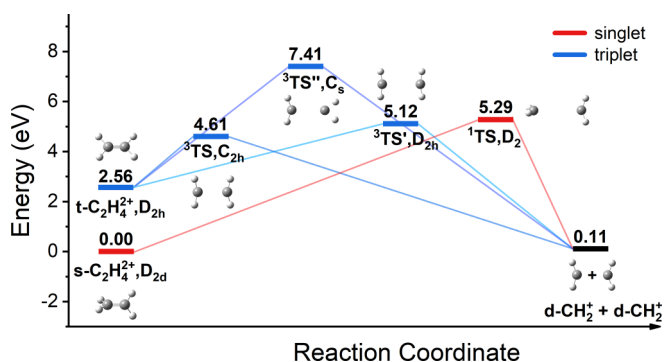


FIG. 4. Potential-energy diagram for the dissociation paths of $\text{C}_2\text{H}_4^{2+} \rightarrow \text{CH}_2^+ + \text{CH}_2^+$. The reactant $\text{C}_2\text{H}_4^{2+}$ ions are in singlet and triplet electronic states and the products, i.e., two CH_2^+ fragments, are both in the doublet state. The relative energies are shown in eV with respect to $\text{C}_2\text{H}_4^{2+}$ in the singlet ground state.

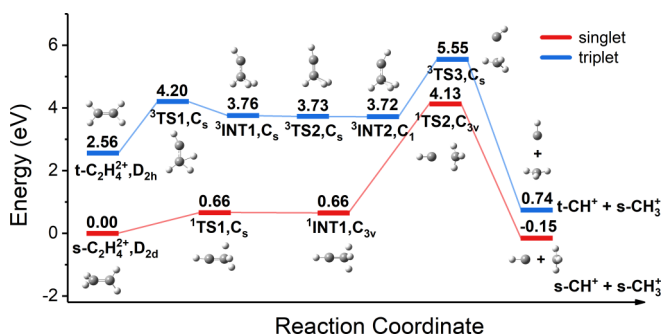


FIG. 5. Potential-energy diagram for the dissociation paths of $C_2H_4^{2+} \rightarrow CH^+ + CH_3^+$. The reactant $C_2H_4^{2+}$ ions are in singlet and triplet electronic states. The CH_3^+ product is in the singlet state, while the other product CH^+ can be in either the singlet or triplet state. The relative energies are shown in eV with respect to $C_2H_4^{2+}$ in the singlet ground state.

twisted D_{2d} symmetry, denoted as $s-C_2H_4^{2+}$. Then $s-C_2H_4^{2+}$ could dissociate into two CH_2^+ fragments in doublet states ($d-CH_2^+$) via the transition state 1TS with a barrier height of 5.29 eV. The reverse activation barrier of this path is 5.18 eV. The structure of $C_2H_4^{2+}$ in the triplet state ($t-C_2H_4^{2+}$) differs from that of $s-C_2H_4^{2+}$ and has a planar D_{2h} geometry. The triplet state is 2.56 eV higher than the ground singlet state. It can proceed with dissociation into two $d-CH_2^+$ fragments in three different paths. Three transition states, i.e., $^3TS'$, $^3TS''$, and $^3TS'''$, are involved, among which the $^3TS''$ transient has an asymmetric structure in C_s symmetry. These paths have different activation barrier energies of 2.05, 2.56, and 4.85 eV, and corresponding reverse activation barriers are 4.50, 5.01, and 7.30 eV, respectively.

As for the $CH^+ + CH_3^+$ channel, a hydrogen transfer process must first occur between the two CH_2 radicals of ethylene to form a methyl group. Therefore, as shown in Fig. 5, the reaction paths of the asymmetric fragmentation are much more complicated than that of the $CH_2^+ + CH_2^+$ channel. One path including two transition states and the other including three transition states are found on the singlet and triplet state PESs, respectively. Subsequent to double ionization, the unstable $s-C_2H_4^{2+}$ undergoes hydrogen-transfer-induced isomerization to form the $[CH - CH_3]^{2+}$ intermediate (denoted as 1INT1) in C_{3v} symmetry via 1TS1 with an activation barrier energy of 0.66 eV. The energies of 1TS1 and 1INT1 are very close, due to a slight structural deformation of hydrogen atoms. Afterwards, the 1INT1 evolves into 1TS2 with the same C_{3v} symmetry and the barrier height is 3.47 eV relative to 1INT1 . During this process, only the distance between the two carbon atoms varies from 1.29 to 2.31 Å. Finally, the 1TS2 dissociates into a singlet $s-CH^+$ ion and a singlet planar $s-CH_3^+$ ion with D_{3h} symmetry, which has a reverse activation energy of 4.28 eV. For the reaction path from the triplet state, $t-C_2H_4^{2+}$ also undergoes a hydrogen-transfer process to form the $[CH - CH_3]^{2+}$ intermediate 3INT1 via a planar transition state 3TS1 with a barrier height of 1.64 eV relative to $t-C_2H_4^{2+}$. Then the internal coordinates of the hydrogen atoms are adjusted to the lower-energy structure of 3INT2 . During this process, the energy of the 3TS2 could be slightly higher than that of 3INT1 without considering the ZPE. But

as shown in Fig. 5, it is 0.03 eV lower after taking the ZPE correction into account, which was also reported in previous studies [34,35]. And this is generally considered to be the result of the fact that the effect of dispersion is ignored in the B3LYP functional. Following the C-C bond breaking of 3INT2 via 3TS3 , fragments of the $t-CH^+$ ion in the triplet state and $s-CH_3^+$ in the singlet state are produced with a reverse activation barrier of 4.81 eV.

The reverse activation barrier energy in a reaction path corresponds to the extra energy of the highest transition state released as the translational energy of products, i.e., KER. The reverse barrier energies of all reaction paths searched for $CH_2^+ + CH_2^+$ and $CH^+ + CH_3^+$ channels are drawn in Fig. 3 as the vertical bars with dashed lines to compare with the measured KER distributions. For the $CH_2^+ + CH_2^+$ channel in Fig. 3(a), the reverse barrier energy from the singlet state is in good agreement with the low-energy KER peak at 5.40 eV, indicating that the path $s-C_2H_4^{2+} \rightarrow d-CH_2^+ + d-CH_2^+$ via 1TS should be a responsible process leading to the low-energy KER. In addition, the blue bars at 5.01 and 7.30 eV for the paths with $^3TS'$ and $^3TS''$ are well consistent with the KER peak values of 5.4 and 7.5 eV. Although the reaction path via 3TS has a reverse barrier of 4.50 eV, which does not match well with the measured KER, it may still contribute to low-energy KER. Thus, in our calculation for the symmetric fragmentation of $C_2H_4^{2+}$, the low-energy KER peak is contributed by the reaction paths in the singlet and triplet states, while the high-energy peak arises from the triplet path via the transition state $^3TS''$ of asymmetric structure. The finding that both the ground and excited states are responsible for the symmetric fragmentation is also obtained in the cases of C_2H_2 and C_2H_6 dications [22,24,27,29]. But unlike the C_2H_6 case involving the hydrogen-transfer process, the present symmetric fragmentation and also the C_2H_2 case have no connection with hydrogen transfer. This is consistent with our expectation that as the number of hydrogen atoms decreases the hydrogen-transfer process is not favored for the symmetric fragmentation of hydrocarbon molecules.

For the asymmetric fragmentation channel $CH^+ + CH_3^+$, as shown in Fig. 3(b), the measured KER distribution presents a single peak of 5.6 eV in the range of 4.0–8.0 eV. This peak value is 0.79 eV higher than the predicted reverse activation energy (4.81 eV) extracted from the reaction path on triplet PES, and 1.32 eV higher than the energy (4.28 eV) from the singlet path. For the reason that a proportion of reactant internal energy in excess of the TS barrier may be converted to additional translational energy of products [36], the predicted reverse barrier energy could be smaller than the experimentally measured KER [23,37]. Besides, if the minimum-energy crossing point occurs between the singlet and triplet state PESs, the available energy of the reverse activation barrier will change to 5.7 eV, which is in good agreement with the experimental result. Therefore, the reaction path on the triplet PES plays an important role in the formation of asymmetric fragmentation. The importance of the excited-state dynamics has also been revealed in the case of $C_2H_6^{2+}$ asymmetric fragmentation [24]. But for the case of $C_2H_2^{2+} \rightarrow C^+ + CH_2^+$ [22,27,30], two contributors are found in the bimodal KER

distribution and thus different excited states are involved. In all of these three cases, the activation energy of the ground-state reaction path is higher (about 1.5 times) than that of the excited-state path [24,27]. This probably results in the experimental forbiddance of the asymmetric fragmentation via hydrogen-transfer-induced isomerization on the PES of the ground state, but occurrence on the PES of the excited state.

IV. CONCLUSIONS

In conclusion, a combined experimental and theoretical study is carried out on the symmetric and asymmetric C-C bond cleavage processes of $C_2H_4^{2+}$ induced by 18-keV/u Ne^{8+} impact. Employing the parameter (i.e., TOF, dissociation angle, and KER) correlation of ionic fragments measured by the COLTRIMS technique, we unambiguously identify two C-C bond cleavage channels, i.e., the dominant one, $C_2H_4^{2+} \rightarrow CH_2^+ + CH_2^+$, and the minor one, $C_2H_4^{2+} \rightarrow CH^+ + CH_3^+$. In order to clarify the dissociation mechanism of the above channels, *ab initio* reaction path calculations are performed for the $C_2H_4^{2+}$ dication both in singlet and triplet electronic states. For the symmetric fragmentation channel $CH_2^+ + CH_2^+$, we obtain one reaction path from the singlet state and three paths from the triplet state. All of these paths exhibit a one-step dissociation with a productlike transition state and involve no hydrogen transfer. These transition states possess different energies and thus could lead to different KERs, which are quite consistent with the peak values of the experimental KER distribution. The high-energy KER peak around 7.5 eV is considered to result from the triplet

state dissociation with a spatially asymmetric transition state $^3TS'$. As for the low-energy KER peak of about 5.4 eV, both the reaction path on the singlet state PES and the other two on the triplet state PES are responsible. For the asymmetric fragmentation channel $CH^+ + CH_3^+$, the KER distribution is unimodal with a peak value of 5.6 eV. A hydrogen-transfer-induced isomerization process is required for this channel to occur. This channel is attributed to the reaction path proceeding on the excited triplet state PES. Such a path has several minima and transition states and exhibits a hydrogen-transfer barrier of 1.64 eV.

This paper shows the importance of hydrogen transfer and excited-state dynamics to the C-C bond cleavage fragmentation of $C_2H_4^{2+}$. But here they do not play the same roles as compared to the cases of $C_2H_2^{2+}$ and $C_2H_6^{2+}$ dissociation [22,24,27,29,30]. Therefore, the present paper, together with previous C_2H_2 and C_2H_6 studies, provides a more comprehensive understanding on the roles of hydrogen transfer, isomerization, and excited state in the dissociation of hydrocarbon molecules.

ACKNOWLEDGMENTS

This work was supported by the National Natural Science Foundation of China under Grants No. U1832201, No. 11874192, and No. 12104185; the National Key Research and Development Program of China under Grant No. 2017YFA0402300; and the Strategic Key Research Program of the Chinese Academy of Sciences under Grant No. XDB34020000.

-
- [1] *Ultrafast Phenomena in Molecular Sciences*, edited by R. de Nalda and L. Bañares, Springer Series in Chemical Physics Vol. 107 (Springer, New York, 2014).
- [2] D. Reiter and R. K. Janev, *Contrib. Plasma Phys.* **50**, 986 (2010).
- [3] M. A. Huels, B. Boudaïffa, P. Cloutier, D. Hunting, and L. Sanche, *J. Amer. Chem. Soc.* **125**, 4467 (2003).
- [4] F. Calegari, D. Ayuso, A. Trabattoni, L. Belshaw, S. De Camillis, S. Anumula, F. Frassetto, L. Poletto, A. Palacios, P. Decleva, J. B. Greenwood, F. Martín, and M. Nisoli, *Science* **346**, 336 (2014).
- [5] A. N. Markevitch, D. A. Romanov, S. M. Smith, and R. J. Levis, *Phys. Rev. Lett.* **92**, 063001 (2004).
- [6] M. Pitzer, M. Kunitski, A. S. Johnson, T. Jahnke, H. Sann, F. Sturm, L. Ph. H. Schmidt, H. Schmidt-Böcking, R. Dörner, J. Stohner, J. Kiedrowski, M. Reggelin, S. Marquardt, A. Schießler, R. Berger, and M. S. Schöffler, *Science* **341**, 1096 (2013).
- [7] R. Schoenlein, L. Peteanu, R. Mathies, and C. Shank, *Science* **254**, 412 (1991).
- [8] O.-H. Kwon and A. H. Zewail, *Proc. Natl. Acad. Sci. USA* **104**, 8703 (2007).
- [9] Y. Zhang, K. de La Harpe, A. A. Beckstead, R. Improta, and B. Kohler, *J. Am. Chem. Soc.* **137**, 7059 (2015).
- [10] R. Dörner, V. Mergel, O. Jagutzki, L. Spielberger, J. Ullrich, R. Moshhammer, and H. Schmidt-Böcking, *Phys. Rep.* **330**, 95 (2000).
- [11] A. Douhal, F. Lahmani, and A. H. Zewail, *Chem. Phys.* **207**, 477 (1996).
- [12] A. Ludwig, E. Liberatore, J. Herrmann, L. Kasmi, P. López-Tarifa, L. Gallmann, U. Rothlisberger, U. Keller, and M. Lucchini, *J. Phys. Chem. Lett.* **7**, 1901 (2016).
- [13] J. van Tilborg, T. K. Allison, T. W. Wright, M. P. Hertlein, R. W. Falcone, Y. Liu, H. Merdji, and A. Belkacem, *J. Phys. B* **42**, 081002 (2009).
- [14] Y. H. Jiang, A. Rudenko, O. Herrwerth, L. Foucar, M. Kurka, K.-U. Kühnel, M. Lezius, M. F. Kling, J. van Tilborg, A. Belkacem, K. Ueda, S. Düsterer, R. Treusch, C. D. Schröter, R. Moshhammer, and J. Ullrich, *Phys. Rev. Lett.* **105**, 263002 (2010).
- [15] E. Wells, C. E. Rallis, M. Zohrabi, R. Siemering, B. Jochim, P. R. Andrews, U. Ablikim, B. Gaire, S. De, K. D. Carnes, B. Bergues, R. de Vivie-Riedle, M. F. Kling, and I. Ben-Itzhak, *Nat. Commun.* **4**, 2895 (2013).
- [16] Y. Boran, G. L. Gutsev, A. A. Kolomenskii, F. Zhu, A. Schuessler, and J. Strohaber, *J. Phys. B* **51**, 035003 (2018).
- [17] P. M. Kraus, M. C. Schwarzer, N. Schirmel, G. Urbasch, G. Frenking, and K.-M. Weitzel, *J. Chem. Phys.* **134**, 114302 (2011).

- [18] N. G. Kling, S. D. Tendero, R. Obaid, M. R. Disla, H. Xiong, M. Sundberg, S. D. Khosravi, M. Davino, P. Drach, A. M. Carroll, T. Osipov, F. Marín, and N. Berrah, *Nat. Commun.* **10**, 2813 (2019).
- [19] S. Maclot, D. G. Piekarski, A. Domaracka, A. Méry, V. Vizcaino, L. Adoui, F. Martín, M. Alcamí, B. A. Huber, P. Rousseau, and S. Díaz-Tendero, *J. Phys. Chem. Lett.* **4**, 3903 (2013).
- [20] S. De, J. Rajput, A. Roy, P. N. Ghosh, and C. P. Safvan, *Phys. Rev. Lett.* **97**, 213201 (2006).
- [21] B. Jochim, A. Lueking, L. Doshier, S. Carey, E. Wells, E. Parke, M. Leonard, K. D. Carnes, and I. Ben-Itzhak, *J. Phys. B* **42**, 091002 (2009).
- [22] Y. Zhang, B. Wang, L. Wei, T. Jiang, W. Yu, R. Hutton, Y. Zou, L. Chen, and B. Wei, *J. Chem. Phys.* **150**, 204303 (2019).
- [23] S. Xu, H. Zhao, X. Zhu, D. Guo, W. Feng, K.-C. Lau, and X. Ma, *Phys. Chem. Chem. Phys.* **20**, 27725 (2018).
- [24] L. Wei, C.-S. Lam, Y. Zhang, B. Ren, J. Han, B. Wang, Y. Zou, L. Chen, K.-C. Lau, and B. Wei, *J. Phys. Chem. Lett.* **12**, 5789 (2021).
- [25] T. Majima, T. Murai, T. Kishimoto, Y. Adachi, S. O. Yoshida, H. Tsuchida, and A. Itoh, *Phys. Rev. A* **90**, 062711 (2014).
- [26] V. V. Afrosimov, A. A. Basalaev, Y. G. Morozov, M. N. Panov, O. V. Smirnov, and E. A. Tropp, *Tech. Phys.* **56**, 597 (2011).
- [27] T. S. Zyubina, Y. A. Dyakov, S. H. Lin, A. D. Bandrauk, and A. M. Mebel, *J. Chem. Phys.* **123**, 134320 (2005).
- [28] A. Mebel and A. Bandrauk, *J. Chem. Phys.* **129**, 224311 (2008).
- [29] B. Gaire, S. Y. Lee, D. J. Haxton, P. M. Pelz, I. Bocharova, F. P. Sturm, N. Gehrken, M. Honig, M. Pitzer, D. Metz, H.-K. Kim, M. Schöffler, R. Dörner, H. Gassert, S. Zeller, J. Voigtsberger, W. Cao, M. Zohrabi, J. Williams, A. Gattton, D. Reedy, C. Nook, T. Müller, A. L. Landers, C. L. Cocke, I. Ben-Itzhak, T. Jahnke, A. Belkacem, and T. Weber, *Phys. Rev. A* **89**, 013403 (2014).
- [30] L. Chen, X. Shan, E. Wang, X. Ren, X. Zhao, W. Huang, and X. Chen, *Phys. Rev. A* **100**, 062707 (2019).
- [31] Y. Zhang, L. Wei, C.-L. Yang, W. Yu, B. Wang, B. Yan, Y. Zou, L. Chen, and B. Wei, *Phys. Rev. A* **100**, 052706 (2019).
- [32] R. T. Zhang, W. T. Feng, X. L. Zhu, S. F. Zhang, D. L. Guo, Y. Gao, D. B. Qian, S. Xu, S. C. Yan, P. Zhang, Z. K. Huang, H. B. Wang, B. Hai, D. M. Zhao, and X. Ma, *Phys. Rev. A* **93**, 032709 (2016).
- [33] M. J. Frisch, G. W. Trucks, H. B. Schlegel, G. E. Scuseria, M. A. Robb, J. R. Cheeseman, G. Scalmani, V. Barone, G. A. Petersson, H. Nakatsuji *et al.*, GAUSSIAN 16 Revision. C.01, Gaussian, Inc., Wallingford, CT, 2016.
- [34] S. Feyel, J. Döbler, R. Hoekendorf, M. K. Beyer, J. Sauer, and H. Schwarz, *Angew. Chem. Int. Ed.* **47**, 1946 (2008).
- [35] E. Wang, X. Ren, W. Baek, H. Rabus, T. Pfeifer, and A. Dorn, *Nat. Commun.* **11**, 2194 (2020).
- [36] F. Zamir and R. D. Levine, *Chem. Phys.* **52**, 253 (1980).
- [37] N. Haag, Z. Berényi, P. Reinhard, D. Fischer, M. Gudmundsson, H. A. B. Johansson, H. T. Schmidt, H. Cederquist, and H. Zettergren, *Phys. Rev. A* **78**, 043201 (2008).